Sensors and Actuators B 248 (2017) 699–707

Contents lists available at ScienceDirect

Sensors and Actuators B: Chemical

journal homepage: www.elsevier.com/locate/snb

# The effect of report particle properties on lateral flow assays: A mathematical model

Zhi Liu [a,b,1], Jie Hu [b,c,1], Ang Li [d], Shangsheng Feng [b], Zhiguo Qu [a,**], Feng Xu [b,c,*]

[a] Key Laboratory of Thermo-Fluid Science and Engineering of Ministry of Education, School of Energy and Power Engineering, Xi'an Jiaotong University, Xi'an 710049, PR China
[b] Bioinspired Engineering and Biomechanics Center (BEBC), Xi'an Jiaotong University, Xi'an 710049, PR China
[c] Key Laboratory of Biomedical Information Engineering of Ministry of Education, School of Life Science and Technology, Xi'an Jiaotong University, Xi'an 710049, PR China
[d] Key Laboratory of Shaanxi Province for Craniofacial Precision Medicine Research and Department of Periodontology, College of Stomatology, Xi'an Jiaotong University, Xi'an 710004, PR China

ARTICLE INFO

*Article history:*
Received 17 December 2016
Received in revised form 28 March 2017
Accepted 5 April 2017
Available online 7 April 2017

*Keywords:*
Lateral flow assays
Convection–diffusion–reaction
Binding site density
Target analyte
Report particle

ABSTRACT

Lateral flow assays (LFAs) have found widespread applications in biomedical fields, but improving their sensitivity remains challenging mainly due to the unclear convection-diffusion-reaction process. Therefore, we developed a 1D mathematical model to solve this process in LFAs. The model depicts the actual situation that one report particle may combine more than one target, which overcomes the deficiency of existing models where one report particle combines only one target. With this model, we studied the effect of report particle characteristics on LFAs, including binding site density, target analyte and report particle concentration. The model was qualitatively validated by reported experimental data and our designed experiments where the report particle with different accessible binding site (HIV-DP) densities is obtained by changing the ratio of HIV-DP and Dengue-DP in preparing AuNP-DP aggregates. The results indicate that a strong signal intensity can be obtained without consuming excess detector probe with the optimum binding site ($\mathbf{N}=30$). A maximum normalized target concentration of 120 is obtained to prevent the false-negative result, while a minimum normalized report particle concentration of 0.015 is recommended to produce a strong signal. The developed model would serve as a powerful tool for designing highly effective LFAs.



## 1. Introduction

Lateral flow assays (LFAs) have shown promising applications in various fields, such as global and public health care [1] and environment monitoring [2], given their cost-effective, convenient, and rapid features. LFAs detect target analytes (*e.g.*, nucleic acid, protein, and cell) in samples through converting them into more easily detectable signals by using report particles with colored (*e.g.*, gold nanoparticles (AuNPs) [3]), luminescent (*e.g.*, upconversion nanoparticles (NPs) [4]), or magnetic ($Fe_3O_4$ NPs [5]) features. Specifically, the target analytes bind with report particles *via* bioreaction forming report particle–analyte complex, which flow *via* diffusion and convection through the test line as induced by the capillary force. The capture probes immobilized in the test line interact with the complex report particle–analytes and form a sandwich format complex (*e.g.*, capture probe–target–report particle). However, LFAs are generally developed empirically and associated with limitation of poor detection sensitivity, mainly due to the lack of understanding of the underlying mechanism of the convection–diffusion–reaction process in LFAs.

Generally, the report particle plays a significant role in the convection–diffusion–reaction process of LFA detection. To enhance detection sensitivity, significant experimental efforts have been put on assessing the effect of report particle characteristics on the LFA performance in the whole convection–diffusion–reaction process, including particle concentration, particle size, and the available binding sites to the target analyte [6]. For instance, the signal from up-converting phosphor particles first increases and then reaches a plateau with increasing particle concentration in detecting single-stranded nucleic acids using LFAs [7]. The detection limit

* Corresponding author at: Bioinspired Engineering and Biomechanics Center (BEBC), Xi'an Jiaotong University, Xi'an 710049, PR China.
** Corresponding author.
*E-mail addresses:* zgqu@mail.xjtu.edu.cn (Z. Qu), fengxu@mail.xjtu.edu.cn, fengxu201@gmail.com (F. Xu).
[1] The authors contributed equally to this work.

http://dx.doi.org/10.1016/j.snb.2017.04.024
0925-4005/

increases with increasing report particle size, however a further increase in particle size has a detrimental effect on the detection limit [8]. Besides, particle size has an important contribution to signal intensity per particle and the maximum number of binding sites on the report particle surface [9]. Accordingly, composite report particles have been developed by coating NPs with chromogenic substance (*e.g.*, enzymes) [10] or linking NPs with other nanomaterials (*e.g.*, AuNP conjugate [11,12], $Fe_2O_3$ NPs [13], and silica nanorods [14]) to increase their size, binding site density, and signal intensity, which in turn improve the detection sensitivity of LFAs. In spite of these experimental advances, the underlying mechanism for the effect of the convection–diffusion–reaction processes on the performance of LFAs remains elusive.

To investigate the underlying mechanism, mathematical and numerical models have been adopted to evaluate the effects of crucial parameters (*e.g.*, concentrations of target analyte, report particle and capture probe) of LFAs. For instance, Qian and Bau introduced mathematical models based on the convection–diffusion–reaction equations to analyze LFAs with sandwich and competitive formats [15,16]. Zeng et al. proposed several algorithms (*e.g.*, extended Kalman filter (EKF) [17], hybrid EKF and the switching particle swarm optimization algorithm [18], particle filter approach [19], and particle swarm optimization method [20]) to simulate and improve the performance of sandwich-type LFAs. However, these existing models assume that one report particle only combines one analyte and neglect the structure of report particle to simplify the bioreactions in LFAs, which deviate from the actual condition where one report particle with numerous accessible binding sites may capture more than one target analyte [9]. Therefore, developing an effective mathematical model based on the real situation is necessary to reveal the effects of report particle with multi-binding sites on the detection result.

In this study, we developed a mathematical model based on the physical law of mass conservation to solve the 1D convection–diffusion–reaction process in LFAs. As the particle size determines the signal intensity, stability, flow characteristic and binding site density of AuNPs, the mathematical study is focused on studying the effects of binding site density and AuNP concentration, which play crucial roles on LFAs detections and can be validated by experiments qualitatively. The model was qualitatively validated by reported experimental data in literature and also our specially designed experiments where the report particles with different accessible binding site (HIV-DP) densities were obtained by changing the ratio of HIV-DP and Dengue-DP in preparing gold nanoparticle (AuNP)-DP aggregates. With this model, we investigated the relationship between report particle and target analyte concentrations, and the LFAs performance. The developed model would provide a physically intuitive illustration of the corresponding experimental results and could help optimize the design of highly sensitive LFAs.

## 2. Materials and methods

### 2.1. Experimental section

#### 2.1.1. Preparation and modification of AuNPs

In the experiment, a nucleic acid of HIV is selected as the target analyte, and a part of its complementary base sequence is the available detector probe (HIV-DP) on AuNP surface. To keep the stability of AuNPs, an abundant detector probe is added to the AuNP solution fully coated on the AuNP surface, forming AuNP-DP aggregates. Therefore, a mixed solution of detector probes, including HIV-DP and Dengue-DP with different mixing proportions, is proposed to investigate the effect of report particle with multiple binding sites. The oligonucleotide sequence (Dengue-DP) doesn't participate in any chemical reactions (Table 1) and is only used to occupy the remainder binding sites on the AuNP surface and to adjust the mixing proportion of HIV-DP in the mixed solution of detector probes in preparing AuNP-DP aggregates.

To achieve different binding site densities, both HIV-DP and Dengue-DP are thiolated and mixed with different proportions to make a mixed detector probe solution. These mixed solutions of detector probes are added to the AuNP solution in different tubes to form AuNP-DPs aggregates with different proportions of HIV-DP. The preparation details are as follows. First, AuNPs with an average diameter of $13 \pm 3$ nm are prepared following the protocol from our previous study [11]. Subsequently, to activate the HIV-DP and to obtain a final concentration of 100 μM, 4 μL of 10 mM TCEP, 20 μL of 500 mM acetate buffer (pH 4.76), and 100 μL of ultrapure water are added to the HIV-DP, while 8 μL of 10 mM TCEP, 39 μL of 500 mM acetate buffer (pH 4.76), and 194 μL of ultrapure water are added to the Dengue-DP to activate the Dengue-DP and to obtain a final concentration of 100 μM. Using the HIV-DP and Dengue-DP, we prepare six mixed detector probe solutions with different HIV-DP/Dengue-DP ratios, namely, 10:0, 8:2, 6:4, 4:6, 2:8, and 10:0, respectively. The six solutions and 5 mL of the prepared AuNP solution are added to six tubes (labeled #1–#6) successively for preparing AuNP-DP conjugates with different binding sites as our previous study [11].

Although the quantitative binding site density is unsure, the different HIV-DP densities of the AuNP-DP conjugate increase with increasing proportions of HIV-DP in the mixed detector probe solutions. Therefore, six different binding site densities on the surface of AuNPs with the same particle size can be obtained by tuning the proportion of HIV-DP in the mixed detector probe solution. A typical proportion of HIV-DP/Dengue-DP (6:4) in the mixed detector probe solution is added to the AuNP solution for an ideal case (Fig. 1c). This figure implies that 60% of the HIV-DP binding sites on AuNP are available to capture the target HIV.

### 2.2. Mathematical model

#### 2.2.1. Development of the model of the convection-diffusion-reaction process in LFAs

The LFA strip mainly comprises three pads (*e.g.*, immersing, detection, and absorption pads) and two lines (*e.g.*, test and control lines) (Fig. 1a). The specific target analyte (**A**) (*e.g.*, oligonucleotide sequence) exists in the sample, and the report particles (**P**) (*e.g.*, AuNPs) are encapsulated in the immersing pad near the side of detection pad. The capture probe (**R**) and the control probe (**C**) are immobilized in the test and control lines in sequence. The detail preparation process of LFA strip is shown in the Supplemental Information.

After the liquid sample with target analyte (**A**) is added to the sample pad, the sample flows to the conjugate pad as driven by capillary force. The report particles (**P**) are dissolved and migrate as fluid flows. In the detection pad, the report particle (**P**) can combine specifically with specific analyte (**A**) based on the complementary base-pairing reactions to form complex (**PA**). The **A** and **PA** further interact with the capture probes (**R**) to form complexes **RA** and **RPA** in the test line, where a red signal appears gradually with accumulation of complex **RPA** (Fig. 1bi). Meanwhile, the remaining report particles will be captured by the control probe (**C**) to form complex **CP** in the control line, where a red signal will also appear with accumulation of **CP**. Once the sample with a certain amount of target analytes is added to the sample pad, the test and control lines appears gradually, indicating a positive result (Fig. 1a). If the target analyte concentration is below the detection limit, only the control line works and the test line does not appear, indicating a negative result. If the control line does not appear, the device fails on account

**Table 1**
Oligonucleotide sequences applied in the current study.

| Name | Sequence |
|---|---|
| HIV-Detector probe (HIV-DP, for detecting target) | 5′-CACAA CAGAC GGGCA CACAC TACT-(CH2)6-HS-3′ |
| Dengue-DP (for protecting AuNPs) | 5′ -HS-(CH2)6-GAGAC AGCAG GATCT CTGGT C-3′ |
| Capture probe | 5′-Biotin/GTCTG AGGGA TCTCT AGTTA CCAG-3′ |
| Control probe | 5′-AGTAG TGTGT GCCCG TCTGT TGTG/Biotin-3′ |
| Target nucleic acid | 5′-AGTAG TGTGT GCCCG TCTGT TGTGT GACTC TGGTA ACTAG AGATC CCTCA GAC-3′ |
| Control nucleic acid | 5′-GCCTC AATAA AGCTT GCCTT GAGTG CTTGT GGAAA ATCTC TAGCA GTGGC GCC-3′ |

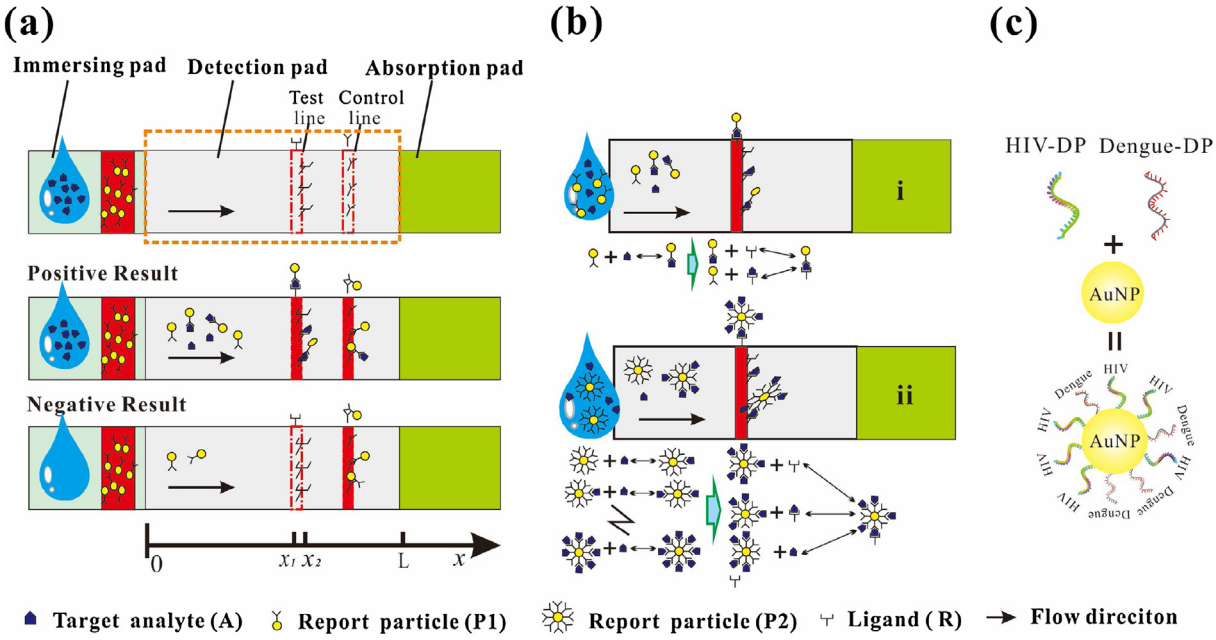


**Fig. 1.** Schematic of the convection-diffusion-reaction progress in LFAs. (a) Schematic of the configuration and measurement principle of LFA; (b) Schematic of the mathematical model with the signal-combining model [15] and Present multi-combining model; (c) Preparation of AuNP-DP aggregates with different percentages of HIV-DP and Dengue-DP.

of the invalid report particle or the inactive control probe. Finally, the waste sample is absorbed and stored in the absorption pad.

Now we consider the actual situation that multiple binding sites are available to combine the target analytes on the surface of report particle (Fig. 1bii). As the dry LFA device comes into contact with the sample solution, the report particle (**P**) starts to react with one or multiple target analytes (**A**) sequentially, forming complex particle–multi-targets $\mathbf{PA}_n$ in the flowing liquid, where **n** is the number of analytes coated on the report particle surface. **A** and $\mathbf{PA}_n$ will then be captured by **R**, forming the complexes capture probe–multi-targets **RA** and particle–multi-targets–capture probe $\mathbf{RPA}_n$ in the test line. The complex **RA** may capture the free **P** and $\mathbf{PA}_n$ with available binding sites to form the complex $\mathbf{RPA}_n$, which with available binding sites, would continue to capture the free **A**. Consequently, the above chemical interactions shown in Fig. 1bii are summarized as

$$\mathbf{A+PA_{n-1}} \underset{k_d}{\overset{k_a}{\leftrightarrow}} \mathbf{PA_n},\ \mathbf{n} = 1, 2, 3, \ldots \mathbf{N}, \tag{1a}$$

$$\mathbf{R+A} \underset{k_d}{\overset{k_a}{\leftrightarrow}} \mathbf{RA}, \tag{1b}$$

$$\mathbf{R+PA_n} \underset{k_d}{\overset{k_a}{\leftrightarrow}} \mathbf{RPA_n},\ \mathbf{n} = 1, 2, 3, \cdots \mathbf{N}, \tag{1c}$$

$$\mathbf{RA+PA_{n-1}} \underset{k_d}{\overset{k_a}{\leftrightarrow}} \mathbf{RPA_n},\ \mathbf{n} = 1, 2, 3, \cdots \mathbf{N}, \tag{1d}$$

$$\mathbf{RPA_{n-1}} + \mathbf{A} \underset{k_d}{\overset{k_a}{\leftrightarrow}} \mathbf{RPA_n},\ \mathbf{n} = 2, 3, 4, \cdots \mathbf{N}, \tag{1e}$$

where $\mathbf{k}_a$ and $\mathbf{k}_d$ are assumed to be the same in these reactions, with $\mathbf{k}_a$ equal to $10^{-3}$ (1/nM s) and $\mathbf{k}_d$ equal to $10^{-3}$ (1/s), corresponding to Qian's research [15]. **N** and **n** are the total accessible binding sites on the surface of report particle and the combined analyte number, respectively. In Eqs. ((1a) and (1e)), when **n** = 1, the term $\mathbf{PA}_{n-1}$ is changed to $\mathbf{PA}_0$, which presents single report particle without target analyte for simplification of the presentation. When **N** equals to 1, the reaction in Eq. (1e) can be neglected. Thus, the chemical reaction processes corresponds to the previous simplified single-combining model (Supplemental information).

The following assumptions are adopted to facilitate establishing the present model. (1) The calculation domain only includes the detection pad, where happens major reactions, as shown by the orange dashed rectangle in Fig. 1a; (2) The target analytes and report particles are dissolved in a buffer solution without reacting before entering the detection pad on account of minimal reaction time on the immersing pad; (3) The liquid flow driven by capillary force is laminar with constant slow speed; (4) The control line is ignored and the report particle will combine with multiple target analytes in sequence.

The concentration–governing equations of the 1D convection–diffusion–reaction model are based on the physical law of mass conservation, which presents the equivalence between the change rate of reagent and the total change rates of diffusion, convection, and source terms. The source term in the

concentration–governing equations is directly determined by the production rates $\boldsymbol{F}_{\mathbf{PA_n}}$, $\boldsymbol{F}_{\boldsymbol{RA}}$, $\boldsymbol{F}_{\mathbf{RPA}_{1,n}}$, $\boldsymbol{F}_{\mathbf{RPA}_{2,n}}$, and $\boldsymbol{F}_{\mathbf{RPA}_{3,n}}$ of complexes $\mathbf{PA}_n$, **RA**, and $\mathbf{RPA}_n$ corresponding to the multi-combining chemical reactions in Eqs. (1a)–(1e) (Supplemental information). Thus, the governing equation of **A** and **P** are given as

$$\frac{\partial \boldsymbol{C}_{\mathrm{A}}}{\partial \boldsymbol{t}} = \boldsymbol{D}_{\mathrm{A}}\frac{\partial^2 \boldsymbol{C}_{\mathrm{A}}}{\partial \boldsymbol{x}^2} - \boldsymbol{U}\frac{\partial \boldsymbol{C}_{\mathrm{A}}}{\partial \boldsymbol{x}} - \left[\boldsymbol{F}_{\mathrm{RA}} + \sum\nolimits_{\mathrm{n}=1}^{\mathrm{N}}\left(\boldsymbol{F}_{\mathrm{PA_n}} + \boldsymbol{F}_{\mathrm{RPA}_{3,\mathrm{n}}}\right)\right]. \quad (2)$$

$$\frac{\partial \boldsymbol{C}_{\mathrm{P}}}{\partial \boldsymbol{t}} = \boldsymbol{D}_{\mathrm{P}}\frac{\partial^2 \boldsymbol{C}_{\mathrm{P}}}{\partial \boldsymbol{x}^2} - \boldsymbol{U}\frac{\partial \boldsymbol{C}_{\mathrm{P}}}{\partial \boldsymbol{x}} - \left(\boldsymbol{F}_{\mathbf{PA_1}} + \boldsymbol{F}_{\mathrm{RPA}_{2,1}}\right). \quad (3)$$

As illustrated in assumptions, the report particle will combine with multiple target analytes in sequence to form $\mathbf{PA}_n$. The concentration–governing equations of complex $\mathbf{PA}_n$ are given as

$$\frac{\partial \boldsymbol{C}_{\mathbf{PA_n}}}{\partial \mathbf{t}} = \boldsymbol{D}_{\mathbf{P}}\frac{\partial^2 \boldsymbol{C}_{\mathbf{PA_n}}}{\partial \mathbf{x}^2} - \boldsymbol{U}\frac{\partial \boldsymbol{C}_{\mathbf{PA_n}}}{\partial \mathbf{x}} + \boldsymbol{F}_{\mathbf{PA_n}} - \boldsymbol{F}_{\mathbf{PA_{n+1}}} - \boldsymbol{F}_{\mathbf{RPA_{n1}}} - \boldsymbol{F}_{\mathbf{RPA}_{2,n+1}}, \mathbf{n} = 1, 2, 3, \cdots \mathbf{N} - 1. \quad (4a)$$

$$\frac{\partial \boldsymbol{C}_{\mathbf{PA_N}}}{\partial \mathbf{t}} = \boldsymbol{D}_{\mathbf{P}}\frac{\partial^2 \boldsymbol{C}_{\mathbf{PA_N}}}{\partial \mathbf{x}^2} - \boldsymbol{U}\frac{\partial \boldsymbol{C}_{\mathbf{PA_N}}}{\partial \mathbf{x}} + \boldsymbol{F}_{\mathbf{PA_N}} - \boldsymbol{F}_{\mathbf{RPA}_{1,N}}. \quad (4b)$$

The balance equation of production rate of **RA** and $\mathbf{RPA}_n$ are given as

$$\frac{\partial \boldsymbol{C}_{\mathrm{RA}}}{\partial \boldsymbol{t}} = \boldsymbol{F}_{\mathrm{RA}} - \sum\nolimits_{\mathrm{n}=1}^{\mathrm{N}}\boldsymbol{F}_{\mathrm{RPA}_{2,\mathrm{n}}}. \quad (5)$$

$$\frac{\partial \boldsymbol{C}_{\mathbf{RPA_n}}}{\partial \mathbf{t}} = \boldsymbol{F}_{\mathbf{RPA_n}}\mathbf{n} = 1, 2, 3, \cdots \mathbf{N}. \quad (6)$$

where $\boldsymbol{C}_{\boldsymbol{A}}$, $\boldsymbol{C}_{\mathbf{PA_n}}$, $\boldsymbol{C}_{\boldsymbol{RA}}$, and $\boldsymbol{C}_{\mathrm{RPA_n}}$ are the concentrations of target analyte and complexes $\mathbf{PA}_n$, **RA**, and $\mathbf{RPA}_n$, respectively; the liquid wicking speed $\boldsymbol{U}$ is 0.2 mm/s, as obtained by experimental method; $\boldsymbol{D}_{\boldsymbol{A}}$ and $\boldsymbol{D}_{\boldsymbol{P}}$ are the diffusion coefficients of target analyte **A** and AuNP **P** and their complexes $\mathbf{PA}_n$, respectively. Accordingly, the diffusion coefficients $\boldsymbol{D}_{\boldsymbol{A}}$ and $\boldsymbol{D}_{\boldsymbol{P}}$ are estimated by using the Stokes–Einstein equation [21] to be $1.0 \times 10^{-10}$ and $1.0 \times 10^{-12}$ $\mathrm{m}^2$/s, respectively. In Eqs. (2)–(6), $\boldsymbol{F}_{\mathrm{RPA}_{3,1}}$ has no corresponding reaction and is supposed to be zero, and $\boldsymbol{F}_{\mathrm{RPA_n}}$ is the total production rate of complex $\mathbf{RPA}_n$.

In the current simulation, the visible signal intensity $\boldsymbol{S}$ is proportional to the total amount of report particle $\boldsymbol{C}_{\boldsymbol{P}}$, conjugates $\boldsymbol{C}_{\mathrm{PA_n}}$, and sandwich forms $\boldsymbol{C}_{\mathrm{RPA_n}}$, namely,

$$\boldsymbol{S} = \boldsymbol{C}_{\mathbf{P}} + \sum \boldsymbol{C}_{\mathbf{PA_n}} + \sum \boldsymbol{C}_{\mathbf{RPA_n}}. \quad (7)$$

Thus, the average signal intensity in the test line can be expressed as

$$\boldsymbol{S}_{\mathbf{ave}} = \int_{\mathbf{x_1}}^{\mathbf{x_2}} \boldsymbol{S}d\boldsymbol{x}/(\mathbf{x_2} - \mathbf{x_1}). \quad (8)$$

Ideally, the effective signal in the test line $\boldsymbol{S}_{\boldsymbol{T}}$ would be proportional to the amount of sandwich format $\mathbf{RPA}_n$, namely,

$$\boldsymbol{S}_{\mathbf{T}} = \int_{\mathbf{x_1}}^{\mathbf{x_2}} \sum \boldsymbol{C}_{\mathbf{RPA_n}} d\boldsymbol{x}/(\mathbf{x_2} - \mathbf{x_1}). \quad (9)$$

#### 2.2.2. Model solution

The mathematical model is discretized by the finite difference method with uniform grid spacing, Fig. S1, and solved with the three-diagonal matrix algorithms (TDMAs) [22]. The solution procedure is illustrated in the supplementary information in detail, Fig. S2.

## 3. Results and discussion

LFAs have found widespread applications in biomedical fields, but improving their sensitivity remains a challenge mainly due to the lack of understanding of the underlying convection–diffusion–reaction process. To address this, we developed a mathematical model based on the physical law of mass conservation to solve the 1D convection–diffusion–reaction process in LFAs (Fig. 1).

### 3.1. Equilibrium time determination

The equilibrium time is the total time for the numerical simulation of the unsteady problem, and thus critical to decide the duration of the signal to reach stable state. To determine the equilibrium time, we investigated three different conditions (*e.g.*, binding site number **N**, concentrations of report particle **P**, and target analyte **A**), Fig. 2. We observed that the signal begins to appear after t = 80 s and sharply increases and reaches a plateau at approximately t = 600 s. This tendency agrees well with the experimental observations that the signal appears until liquid front reaches the test line and increases with the reaction progress to achieve a stable state. As for the effect of binding site number **N** (1, 5, 10, 20), the signal is significantly enhanced when **N** > 1 in the steady stage, but is not sensitive to **N** when **N** > 5 (Fig. 2a). The signal is sensitive to report particle and target analyte concentration at t = 600 s (Fig. 2b–c) when the capture capability is saturated. The most intensified signal is obtained at $\boldsymbol{C}_{\mathbf{P0}}$ = 10 nM and $\boldsymbol{C}_{\mathbf{A0}}$ = 10 nM. Therefore, the equilibrium time of 600 s is selected as the signal acquisition time for the following studies.

#### 3.1.1. Effect of binding site densities on report particle on LFA performance

Considering the significant role of binding site densities of report particle, we performed both simulation and experimental studies to investigate the effect of binding site density on the performance of LFAs (Fig. 3). The image of experimental result with different percentages of HIV-DP in preparing AuNP-DP conjugates is shown in Fig. 3a. The target analyte concentrations are selected as 1/10/100 nM in the experiment. The signal in the test line increases at the initial stage and then shows no significant change with further increase of HIV-DP percentage for a constant target analyte concentration. At a fixed percentage of HIV-DP, a strong signal can be obtained at a high target HIV concentration. On the contrary, the signal in the control line increases with increasing percentage of HIV-DP because the AuNP-DP conjugates with a large percentage of HIV-DP (which is complementary to the control probe) can be easily captured in the control line.

To validate the model, we qualitatively compared the simulation results with the experimental data. Since the signal is linear proportional to the accumulated report particles in test zone [15], the signal intensities are normalized as following for convenient comparison. The signal intensity $\boldsymbol{S}_{\mathrm{T\text{-}exp}}$ from experiments can be obtained by quantifying the color density using the ImageJ software, and it is further converted to a normalized form. The maximum signal intensity $\boldsymbol{S}^{\mathrm{max}}_{\mathrm{T\text{-}exp}}$, which corresponds to 80% of the HIV-DP percentage when the target analyte concentration is 100 nM, is selected as reference intensity. The obtained optical signals $\boldsymbol{S}_{\mathrm{T\text{-}exp}}$ are normalized to $\boldsymbol{S}^{\mathrm{max}}_{\mathrm{T\text{-}exp}}$ and defined as

$$\boldsymbol{NS}_{\mathrm{exp}} = \boldsymbol{S}_{\mathrm{T\text{-}exp}}/\boldsymbol{S}^{\mathrm{max}}_{\mathrm{T\text{-}exp}}. \quad (10)$$

Similarly, the target analyte concentration $\boldsymbol{C}_{\mathbf{Ar\text{-}exp}}$ = 1 nM is selected as the reference value. Therefore, the normalized analyte concentration $\boldsymbol{C}_{\mathbf{A0\text{-}exp}}/\boldsymbol{C}_{\mathbf{Ar\text{-}exp}}$ is 1/10/100, which is the ratio between the experimental target concentration

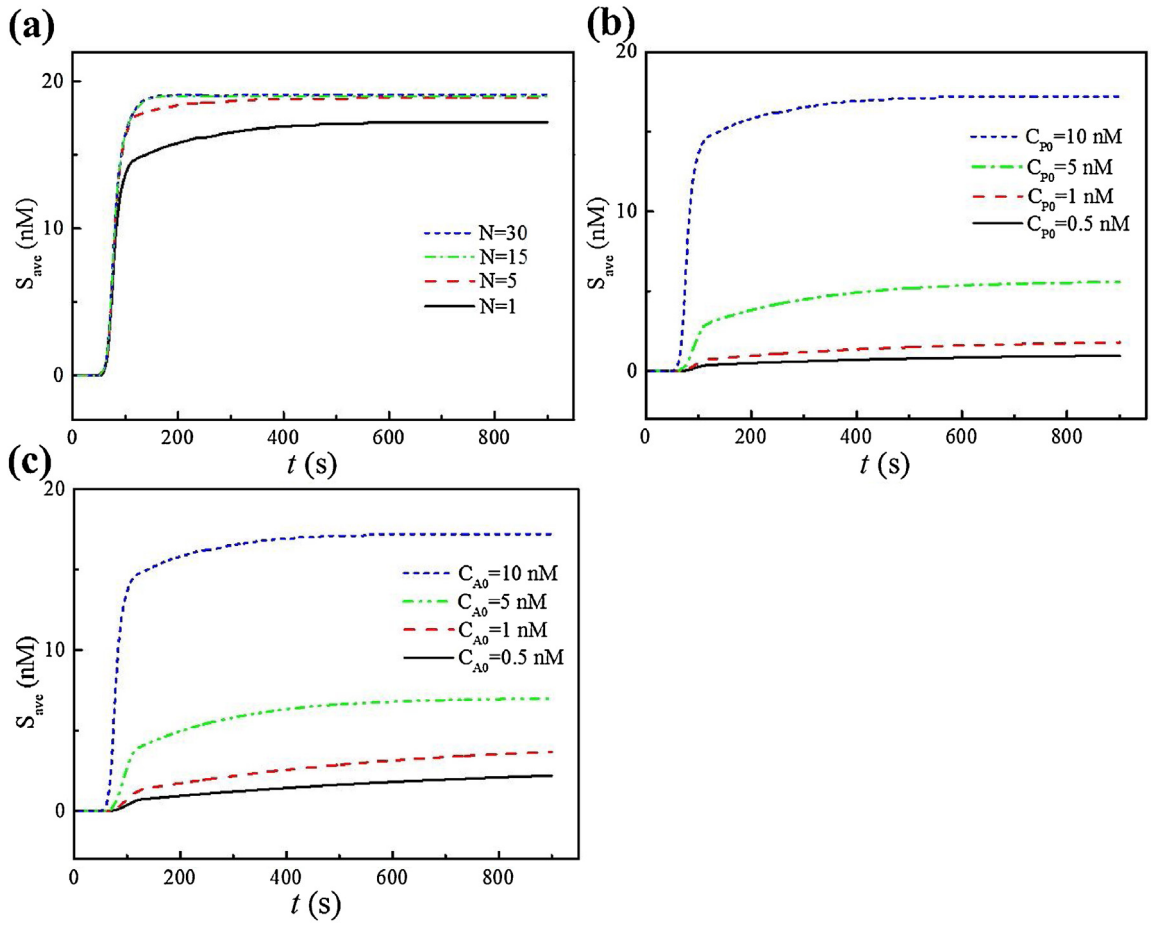


**Fig. 2.** Relationship between average signal $S_{ave}$ and assay time. (a) Average signal for different binding numbers **N**; (b) Average signal for different report particle concentrations at **N** = 1; (c) Average signal for different target analyte concentrations at **N** = 1.

($C_{A0\text{-}exp}$ = 1/10/100 nM) and $C_{Ar\text{-}exp}$. Correspondingly, the maximum simulation signal $S_T^{max}$ calculated in Eq. (9), which corresponds to **N** = 60 and $C_{A0}$ = 10 nM, is defined as reference signal. The normalized signal, which is the ratio between simulation signal and $S_T^{max}$, is expressed as

$$NS = S_T / S_T^{max}. \quad (11)$$

The target analyte concentration $C_{Ar}$ = 0.1 nM is selected as the reference value. The normalized analyte concentration $C_{A0}/C_{Ar}$ is 1/10/100 nM, which is obtained through dividing analyte concentration ($C_{A0}$ = 0.1/1/10 nM) by $C_{Ar}$. The increasing tendency of experimental normalized signal is in good agreement with that of simulation normalized signal (Fig. 3b). The simulation signal increases at the initial stage with increasing **N** and reaches a plateau at **N** = 30. In addition, the signal increases with increasing target HIV concentration at fixed **N** = 30.

Before **N** = 30, the combining capacity between the AuNP-DP conjugate and the target analyte increases with increasing binding sites according to Eq. (S2). The AuNP-DP conjugates with large **N** can combine with considerable target analytes to form complex $PA_n$ with many analytes (large **n**), which will increase the amount of complex $PA_n$ and reduce the amount of free target analyte in liquid. As a result, the complex $PA_n$ is more competitive to be captured by the capture probes in the test zone than the free analyte, resulting in a stronger signal. By contrast, the free target analytes reduce to low levels after the signal reaches the plateau. This competitive effect between free target analyte and complex $PA_n$ results in that the combining capacity and the amount of $PA_n$ change narrowly at **N** > 30.

To verify the analysis, we gives an intuitive illustration that the total amount of concentration of complex $C_{PA_n}$ ($\sum_{n=1}^{N} C_{PA_n}$) increases with increasing binding density before **N** = 30 (Fig. 3c). An insensitive increase with further increasing binding density is then observed, which in turn causes the relative signal to hit a plateau. All these results indicate an optimum binding site density of report particle (**N** = 30 in simulation), which may reduce consuming excess detector probe in preparing AuNP-DP conjugates and provide an excellent performance of LFA.

### 3.2. Performance of LFAs with different target analyte concentrations

To give a better guidance for the experimental research, we further investigated the effects of target analyte concentration on the performance of LFAs by using report particles with different binding site densities (Fig. 4). A normalized intensity *NS* is obtained by Eq. (11), in which the maximum simulation signal *ST* max is selected when $C_{A0}$ = 20 nM and **N** = 30. The normalized target concentration $C_{A0}/C_{Ar}$ is calculated corresponding to that in Fig. 3c, and the reference target concentration is $C_{A0}$ = 0.1 nM. We found that the normalized signal intensities for the four different binding site densities (**N** = 1, 5, 15, 30) all increase linearly to a peak value and then decrease with increasing $C_{A0}/C_{Ar}$ (Fig. 4a). The normalized target concentration $C_{A0}/C_{Ar}$ corresponding to the peak signal value is approximately 120. When $C_{A0}/C_{Ar}$ is below 120, the increas-

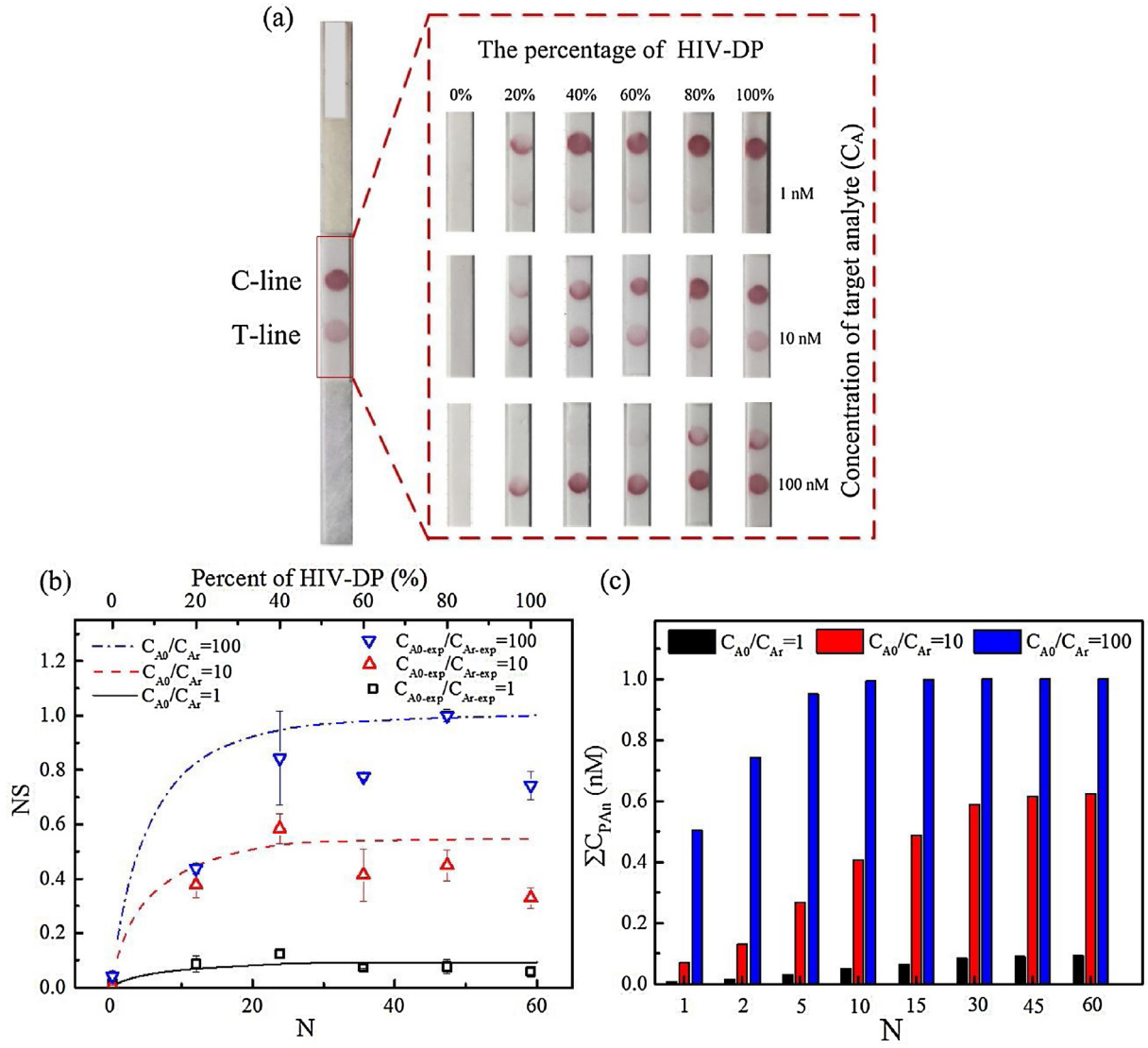


**Fig. 3.** Validation and prediction of the model with different binding site densities. (a) Experimental results using different percentages of HIV-DP in preparing AuNP-DP conjugates; (b) Comparison between the experimental-normalized signal and simulation-normalized signal as a function of binding site number; (c) Simulation results of the amount of complex $\boldsymbol{C}_{\mathbf{PAn}}$ ($\sum_{n=1}^{N}\boldsymbol{C}_{\mathbf{PAn}}$) as a function of binding site **N**.

ing tendency appears with increasing $\boldsymbol{C}_{\mathbf{A0}}/\boldsymbol{C}_{\mathbf{Ar}}$ because the complex $\mathbf{PA}_n$, which increases with increasing free target analyte, plays a dominant role in competition with free target analyte in binding to capture probes in the test line. A further decreasing tendency is found to be associated with increasing $\boldsymbol{C}_{\mathbf{A0}}/\boldsymbol{C}_{\mathbf{Ar}}$ because excess free target analyte competes with complex $\mathbf{PA}_n$ to bind to capture probes in the test line, which hinders the complex $\mathbf{PA}_n$ from reacting with capture probes and causes a false-negative result. This finding implies that the signal intensity can be augmented in some particular range of target analyte concentration, and the increment tendency (Fig. 4c) is only within the range when the normalized target analyte concentration is below 120. The predicted tendency in Fig. 4(a) is consistent with the experimentally reported "hook effect" [23]. In addition, a larger binding site density produces a stronger signal for a constant target HIV concentration, and the increment gradually becomes weak around $\mathbf{N} = 30$, when $\boldsymbol{C}_{\mathbf{A0}}/\boldsymbol{C}_{\mathbf{Ar}}$ is smaller than 100. This tendency also agrees well with that in Fig. 3a. The hook effect in Fig. 4a gives guidance for the valid detection range of the target for the rising stage and prevents a false-negative result in the decreasing stage.

The curve slope for *NS* below the peak signal intensity, as shown in Fig. 4a, is defined as $\mathbf{b}_A$ [$\log(\boldsymbol{NS}) \propto \mathbf{b}_A \log(\boldsymbol{C}_{\mathbf{A0}}/\boldsymbol{C}_{\mathbf{Ar}})$]. Fig. 4b presents that $\mathbf{b}_A$ decreases with increasing binding site density, indicating that a high binding site density may produce a low rate of signal response to the target analyte. As shown in Fig. 4c, the peak target analyte concentration $\boldsymbol{C}_{\mathrm{A_{peak}}}$ corresponding to the peak signal in Fig. 4a shows an augmented tendency with increased binding site density, resulting in a wide detection range for the rising stage. Therefore, a relatively higher binding site density could be used in preparing AuNP aggregates to obtain a more appropriate signal response and to achieve a wider detection range.

We performed a qualitative comparison between the current simulation for different binding site densities and the experimental results of Corstjens et al. [7] and Oh et al. [23] (Fig. 4d). The dimensionless signal $\boldsymbol{NS}$ is obtained when the maximum signal intensity is selected as $S_T^{max}$ for simulations and experiments at each case. A dimensionless target analyte concentration $\boldsymbol{C}_{\mathbf{A0}}/\boldsymbol{C}_{\mathbf{A_{peak}}}$ is in x-axis, where the reference $\boldsymbol{C}_{\mathrm{A_{peak}}}$ is the peak target analyte concentration corresponding to $\boldsymbol{S}_T^{max}$ for each case. A similar "hook effect" in Fig. 4a is identified at various bounding densities, and this trend agrees

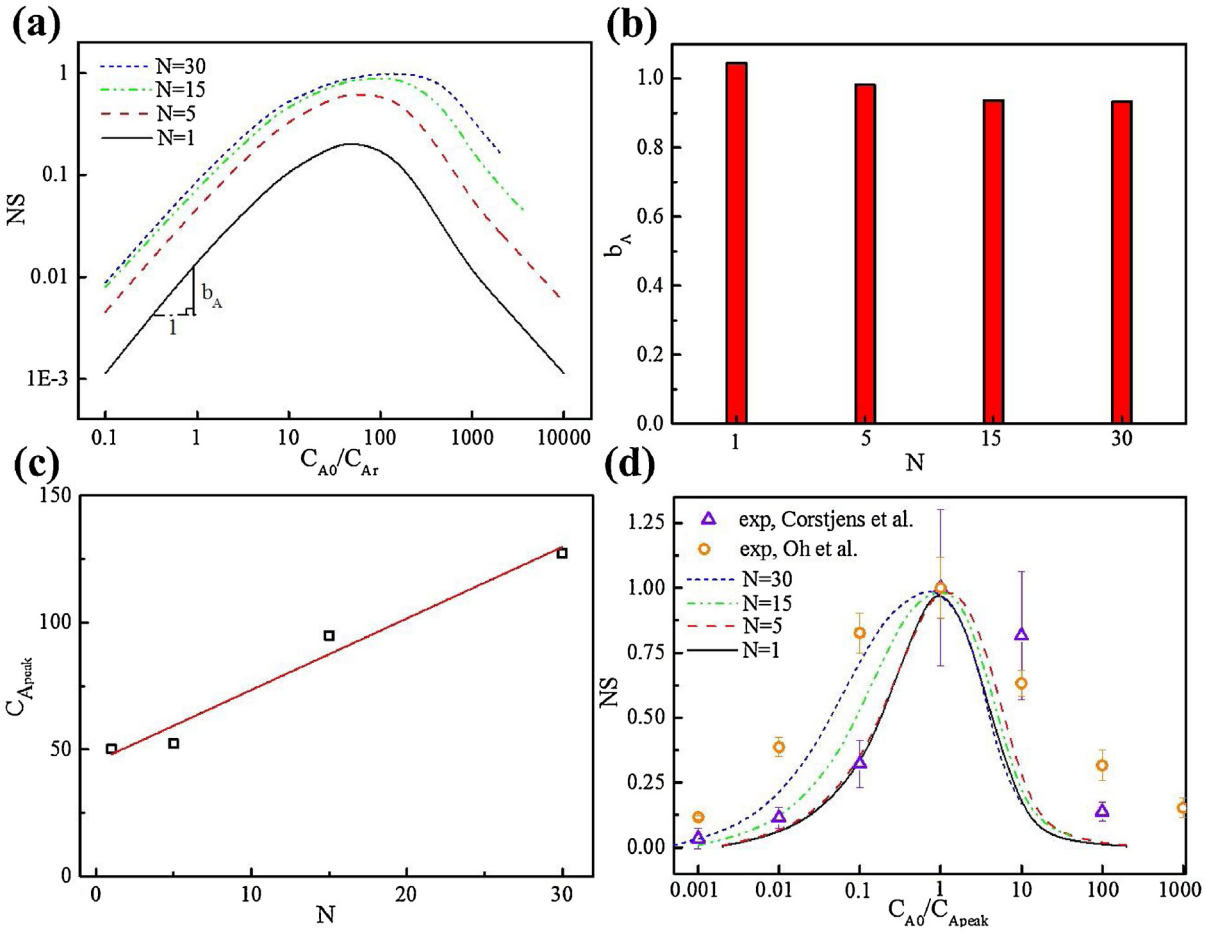


**Fig. 4.** Relationship between target analyte concentration and the performance of LFAs. (a) Effect of the target analyte concentration on the effective signal $S_T$; (b) Slope $b_A$ as a function of the binding site **N**; (c) Peak target analyte concentration $C_{A_{peak}}$ as a function of the binding site **N**; (d) Comparison of the dimensionless signal to target analyte between simulation result and experimental data from Refs. [7,23].

well with the experimental data. Therefore, the present model is further validated with the predicted hook effect tendency.

### 3.3. Optimization of report particle concentration

One of the most crucial factors in manufacturing LFAs is the report particles encapsulated in the immersing pad. To investigate this parameter, we checked the performance of LFAs with different report particles at four binding site densities (Fig. 5). A normalized intensity ***NS*** is obtained by Eq. (11), in which the maximum simulation signal $S_T^{max}$ is selected at $C_{P0}$ = 20 nM and **N** = 30. $C_{Pr}$ = 100 nM is selected as a reference value; thus, the normalized report particle concentration $C_{P0}/C_{Pr}$ can be obtained. The *NS* at four binding site numbers (**N** = 1, 5, 15, 30) first increases linearly and then reaches a plateau value with increasing $C_{P0}/C_{Pr}$ (Fig. 5a). These results are attributed to the following reason. More production of complex $PA_n$ in the flowing liquid is acheived when the report particle concentration is enhanced at the initial stage, resulting in higher sensitivity of LFAs. By contrast, the capture capacity of capture probe in the test line is saturated with further increase of report particle concentration and no further increase in the detection signal. ***NS*** also increases with increasing binding site density in the linearly increasing stage.

Similarly, the slope for ***NS*** below the plateau value of signal intensity is defined as $b_P$ [$\log(NS) \propto b_P \log(C_{P0}/C_{Pr})$](Fig. 5a). $b_P$ decreases narrowly with increasing **N** (Fig. 5b), indicating that the binding site density has a mild effect on the rate of signal increase below the plateau value. The minimum normalized report particle concentration $C_{Pmin}$ is selected when ***NS*** is approximately 5% less than the maximum normalized signal (the inset of Fig. 5a). Obviously, $C_{Pmin}$ decreases with increasing binding site density (Fig. 5c). However, once the binding site number exceeds a certain value (**N** = 10), the decreasing tendency of $C_{Pmin}$ becomes insensitive. When **N** = 30, the value of $C_{Pmin}$ is approximately 0.015. Thus, a reasonable report particle concentration can be obtained to achieve a strong signal intensity and to reduce the waste of reagent AuNP-DP in experimental research. Similarly, a relationship between the dimensionless signal ***NS*** and the dimensionless report particle concentration $C_{P0}/C_{Pr}$ is obtained to compare qualitatively with the experimental results of Corstjens et al. [7] (Fig. 5d). The dimensionless signal ***NS*** is obtained for each case, but the maximum signal intensity is selected as $S_T^{max}$ for each case, including simulations and experiment. A dimensionless report particle concentration $C_{P0}/C_{Pmin}$ is in x-axis, where the reference$C_{Pmin}$ represents the minimum report particle concentration when the signal reaches the plateau for each case. The predicted results of the model with different binding sites present a similar tendency that the dimensionless signal first increases and then reaches a plateau with increasing $C_{P0}/C_{Pmin}$, which agrees well with the experimental data of Corstjens [7] and verifies the current mathematical model.

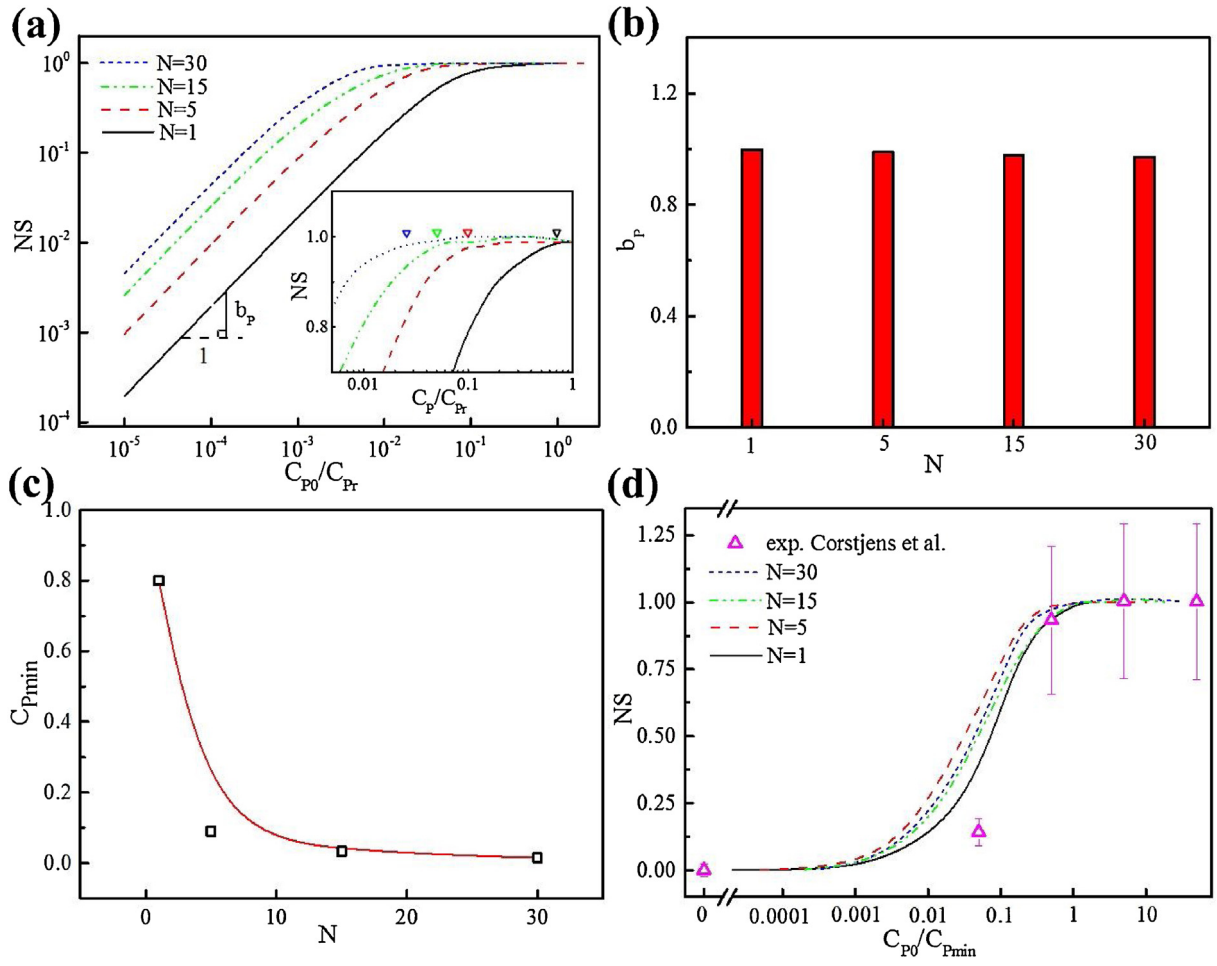


**Fig. 5.** Performances of LFAs with different report particle concentrations. (a) Effect of the report particle concentration on the effective signal $S_T$; (b) Slope $b_P$ as a function of the binding site **N**; (c) Minimum report particle concentration $C_{P_{min}}$ as a function of the binding site **N**; (d) Comparison of the dimensionless signal to report particle between simulation result and experimental data from Ref. [7].

## 4. Conclusions

A mathematical model based on one report particle with multiple binding sites is proposed to analyze the effect of the properties of report particle on the performance of LFAs. The model results are qualitatively validated by comparing the normalized signal with our specially designed experiments and the reported experimental data from literature. An optimum signal intensity is obtained when **N** = 30. The increasing tendency of signal intensity becomes weak when **N** > 30. The normalized signal intensity first increases and then decreases with increasing normalized target concentration. The strongest normalized peak signal is obtained when $C_{A0}/C_{Ar}$ = 120 and **N** = 30. The false-negative result can be effectively prevented according to the guidance of hook effect when $C_{A0}/C_{Ar}$ < 120. A minimum normalized report particle concentration $C_{Pmin}$ exists to guarantee strong signal intensity. $C_{Pmin}$ decreases with increasing **N**.

In this study, we focus on investigating the effects of properties of report particles on the performance of LFAs. The developed model also can be extended by considering the varying liquid flowing behavior in modified structures of LFAs to analyze relationships among the modified structure, liquid flowing field and detection signal. We envision that the mathematical model could give an optimization of LFAs design.

## Acknowledgments

This work was financially supported by the National Natural Science Foundation of China (51322604), the National Program for Support of Top-notch Young Professionals, the National Instrumentation Program (2013YQ190467), and the Fundamental Research Funds for the Central Universities.

## Appendix A. Supplementary data

Supplementary data associated with this article can be found, in the online version, at http://dx.doi.org/10.1016/j.snb.2017.04.024.

## References

[1] J. Hu, S. Wang, L. Wang, F. Li, B. Pingguan-Murphy, T.J. Lu, et al., Advances in paper-based point-of-care diagnostics, Biosens. Bioelectron. 54 (2014) 585–597.
[2] C.-H. Chao, C.-S. Wu, C.-C. Huang, J.-C. Liang, H.-T. Wang, P.-T. Tang, et al., A rapid and portable sensor based on protein-modified gold nanoparticle probes and lateral flow assay for naked eye detection of mercury ion, Microelectron. Eng. 97 (2012) 294–296.
[3] W. Zhou, X. Gao, D. Liu, X. Chen, Gold nanoparticles for in vitro diagnostics, Chem. Rev. 115 (2015) 10575–10636.
[4] X. Ge, A.M. Asiri, D. Du, W. Wen, S. Wang, Y. Lin, Nanomaterial-enhanced paper-based biosensors, TrAC Trend Anal. Chem. 58 (2014) 31–39.
[5] C. Liu, Q. Jia, C. Yang, R. Qiao, L. Jing, L. Wang, et al., Lateral flow immunochromatographic assay for sensitive pesticide detection by using Fe3O4 nanoparticle aggregates as color reagents, Anal. Chem. 83 (2011) 6778–6784.

[6] J. Bailes, S. Mayoss, P. Teale, M. Soloviev, Gold nanoparticle antibody conjugates for use in competitive lateral flow assays, in: M. Soloviev (Ed.), Nanoparticles in Biology and Medicine, Humana Press, Totowa, New Jersey, 2012, pp. 45–55.
[7] P.L.A.M. Corstjens, M. Zuiderwijk, M. Nilsson, H. Feindt, R. Sam Niedbala, H.J. Tanke, Lateral-flow and up-converting phosphor reporters to detect single-stranded nucleic acids in a sandwich-hybridization assay, Anal. Biochem. 312 (2003) 191–200.
[8] M.P.A. Laitinen, M. Vuento, Affinity immunosensor for milk progesterone: identification of critical parameters, Biosens. Bioelectron. 11 (1996) 1207–1214.
[9] I. Safenkova, A. Zherdev, B. Dzantiev, Factors influencing the detection limit of the lateral-flow sandwich immunoassay: a case study with potato virus X, Anal. Bioanal. Chem. 403 (2012) 1595–1605.
[10] C. Parolo, A. de la Escosura-Muñiz, A. Merkoçi, Enhanced lateral flow immunoassay using gold nanoparticles loaded with enzymes, Biosens. Bioelectron. 40 (2013) 412–416.
[11] J. Hu, L. Wang, F. Li, Y.L. Han, M. Lin, T.J. Lu, et al., Oligonucleotide-linked gold nanoparticle aggregates for enhanced sensitivity in lateral flow assays, Lab Chip 13 (2013) 4352–4357.
[12] D.H. Choi, S.K. Lee, Y.K. Oh, B.W. Bae, S.D. Lee, S. Kim, et al., A dual gold nanoparticle conjugate-based lateral flow assay (LFA) method for the analysis of troponin I, Biosens. Bioelectron. 25 (2010) 1999–2002.
[13] D. Tang, J.C. Sauceda, Z. Lin, S. Ott, E. Basova, I. Goryacheva, et al., Magnetic nanogold microspheres-based lateral-flow immunodipstick for rapid detection of aflatoxin B2 in food, Biosens. Bioelectron. 25 (2009) 514–518.
[14] H. Xu, J. Chen, J. Birrenkott, J.X. Zhao, S. Takalkar, K. Baryeh, et al., Gold-nanoparticle-decorated silica nanorods for sensitive visual detection of proteins, Anal. Chem. 86 (2014) 7351–7359.
[15] S. Qian, H.H. Bau, A mathematical model of lateral flow bioreactions applied to sandwich assays, Anal. Biochem. 322 (2003) 89–98.
[16] S. Qian, H.H. Bau, Analysis of lateral flow biodetectors: competitive format, Anal. Biochem. 326 (2004) 211–224.
[17] N. Zeng, Z. Wang, Y. Li, M. Du, X. Liu, Inference of nonlinear state-space models for sandwich-type lateral flow immunoassay using extended kalman filtering, IEEE Trans. Bio-Med. Eng. 58 (2011) 1959–1966.
[18] N. Zeng, W. Zidong, L. Yurong, D. Min, L. Xiaohui, A hybrid EKF and switching PSO algorithm for joint state and parameter estimation of lateral flow immunoassay models, IEEE ACM Trans. Comput. BI 9 (2012) 321–329.
[19] N. Zeng, Z. Wang, Y. Li, M. Du, X. Liu, Identification of nonlinear lateral flow immunoassay state-space models via particle filter approach, IEEE Trans. Nanotechnol. 11 (2012) 321–327.
[20] N. Zeng, Y.S. Hung, Y. Li, M. Du, A novel switching local evolutionary PSO for quantitative analysis of lateral flow immunoassay, Expert Syst. Appl. 41 (2014) 1708–1715.
[21] J. McGrath, M. Jimenez, H. Bridle, Deterministic lateral displacement for particle separation: a review, Lab Chip 14 (2014) 4139–4158.
[22] Z.G. Qu, W.Q. Li, J.J. Zhang, W.Q. Tao, Numerical study of heat conduction with a chemical reaction at the moving frontal surface for a graphite plate, Numer. Heat Transf. Part A: Appl. 67 (2015) 189–209.
[23] Y.K. Oh, H.-A. Joung, H.S. Han, H.-J. Suk, M.-G. Kim, A three-line lateral flow assay strip for the measurement of C-reactive protein covering a broad physiological concentration range in human sera, Biosens. Bioelectron. 61 (2014) 285–289.

## Biographies

**Zhi Liu** was born in P.R. China. He received the B.E. degree from Huazhong University of Science and Technology, Wuhan, China in 2012, and now is pursuing the Ph.D. degree of School of Energy and Power Engineering in Xi'an Jiaotong University, Xi'an, Shaanxi, China. His work focuses on studying the flow mechanism in paper-based diagnosed devices.

**Jie Hu** was born in P.R. China. He received his B.E. from Xi'an Jiaotong University, Xi'an, China in 2011. He was a visiting scholar at Washington University in St. Louis, USA during 2015, and is now pursuing the Ph.D. degree of biomedical engineering in Xi'an Jiaotong University. His work focuses on the research and development of point-of-care technologies.

**Ang Li** was born in P.R. China. He received his B.S. in College of Stomatology from Xi'an Jiaotong University, and M.S. in College of Stomatology from China Medical University at Shenyang, and his Ph.D. in College of life Science and Technology from Xi'an Jiaotong University. Dr. Li's current research interests are paradontosis vaccine of Porphyromonas gingivalis and stomatology technology.

**Shangsheng Feng** was born in P.R. China. He received his B.S. in marine engineering from Wuhan University of Technology, and his Ph.D. in thermal fluid from Xi'an Jiaotong University. Currently, Dr. Feng is a lecturer at School of Aerospace, Xi'an Jiaotong University. Dr. Feng's current research interests are flow transport in paper-based microfluidics, and thermal management of electronics and LEDs.

**Zhi Guo Qu** was born in P.R. China. He received the B.S. and Ph.D. degrees in School of Energy and Power Engineering from Xi'an Jiaotong University. Currently, Dr. Qu is a full professor at School of Energy and Power Engineering, Xi'an Jiaotong University. Dr. Qu's main research interests are heat and mass transfer in porous material, thermophysics in biomedicine and energy saving and emission reduction technology.

**Feng Xu** was born in P.R. China. He received his B.S. in both Thermal & Power Engineering and Industry Engineering and M.S. in Mechanical Engineering from Xi'an Jiaotong University, and his Ph.D. in Engineering from Cambridge University. He worked as a research fellow at Harvard Medical School and Harvard-MIT Health Science & Technology (HST). Currently, Dr. Xu is a full professor at School of Life Science and Technology, Xi'an Jiaotong University. Dr. Xu's current research aims at advancing human health through academic excellence in education and research that integrates engineering, science, biology and medicine with focus on Bio-thermo-mechanics, Engineering of Cell Microenvironment, and Point-of-Care Technologies.